frontiers | Frontiers in Chemistry

TYPE Original Research
PUBLISHED 05 October 2022
DOI 10.3389/fchem.2022.1020484

OPEN ACCESS

EDITED BY
Shijie Li,
Zhejiang Ocean University, China

REVIEWED BY
Yanping Liu,
Zhejiang Ocean University, China
Xiaofeng Shen,
Zhejiang University of Science and Technology, China

*CORRESPONDENCE
Muhammad Idrees,
m.idrees8223@gmail.com
Guijun Li,
gliad@connect.ust.hk

SPECIALTY SECTION
This article was submitted to Photocatalysis and Photochemistry, a section of the journal Frontiers in Chemistry

RECEIVED 18 August 2022
ACCEPTED 20 September 2022
PUBLISHED 05 October 2022

CITATION
Gull S, Batool S, Li G and Idrees M (2022), Synthesis of cesium lead halide perovskite/zinc oxide ($CsPbX_3$/ZnO, X= Br, I) as heterostructure photocatalyst with improved activity for heavy metal degradation.
Front. Chem. 10:1020484.
doi: 10.3389/fchem.2022.1020484

Synthesis of cesium lead halide perovskite/zinc oxide ($CsPbX_3$/ZnO, X= Br, I) as heterostructure photocatalyst with improved activity for heavy metal degradation

Sehrish Gull[1], Saima Batool[2,3], Guijun Li[1]* and Muhammad Idrees[4,3]*

[1]Key Laboratory of Optoelectronics Devices and Systems of Ministry of Education, College of Physics and Optoelectronic Engineering, Shenzhen University, Shenzhen, China, [2]Institute for Advanced Study, Shenzhen University, Shenzhen, China, [3]Institute of Microscale Optoelectronics, Shenzhen University, Shenzhen, China, [4]Additive Manufacturing Institute, College of Mechatronics and Control Engineering, Shenzhen University, Shenzhen, China

Inorganic perovskites have been recognized as highly potent materials for the display and medical industries due to their outstanding features. However, there haven't been many reports on their implications as a photocatalyst for the removal of heavy metals. Photocatalysis has been regarded as a significant approach for the removal of pollutants because of its great sustainability, improved efficiency, and reduced energy consumption. Here, we applied inorganic cesium lead halides (Br and I) with zinc oxide heterostructure as a photocatalyst for the first time. The heterostructure has been synthesized by the traditional hot injection strategy and its photocatalytic activity was systematically investigated. Interestingly, the $CsPbX_3$/ZnO heterostructure as a photocatalyst has a homogeneous geometry and possesses an excellent degradation efficiency of over 50% under xenon UV-Visible light. The $CsPbX_3$/ZnO catalyst carries superior oxidation/reduction properties and ionic conductivity due to the synergistic photogenerated charge carrier and interaction between $CsPbX_3$ and ZnO. The recycling experiment showed the good stability of the catalysts. These findings suggest that inorganic lead halide heterostructure has the potential to be used for heavy metal degradation and water pollution removal catalysts.

KEYWORDS

cesium lead halide/zinc oxide, heterostructure, hot injection strategy, photocatalyst, degradation

1 Introduction

Lead tri-halide perovskites have been considered as a fascinating class of materials for next generation applications due to their remarkable characteristics, including enhanced optical features, high extinction constant, tunable bandgap, versatile surface chemistry, long-range electron-hole diffusion, and high carrier mobility (Akkerman et al., 2015; Gull et al., 2020). This class of materials possesses the general formula of ABX_3 where A is a cation (organic/inorganic), B is a divalent metal (Pb^{2+}, Sn^{2+}, Ge^{2+}), and X is an anion (Cl^{1-}, Br^{1-}, I^{1-} or mixture) (Kulkarni et al., 2019; Yang et al., 2019). In recent years, semiconductor materials have been widely used as photocatalyst in the environmental and energy sectors due to their novel physiochemical features and cost-effectiveness (Batool et al., 2020; Shen et al., 2021b) Commonly used metal-based semiconducting photocatalysts include TiO_2 (Fujishima et al., 2000) (Zhang et al., 2021b), Fe_2O_3 (Hitam and Jalil, 2020), CdS (Cheng et al., 2018), MoS_2 (Shen et al., 2020), ZnS (Lee and Wu, 2017), and ZnO (Johar et al., 2015).

Zinc Oxide (ZnO) has a bandgap of 3.37 eV and can treat heavy metals due to its high photocatalytic efficiency and excitation binding energy-producing electron-hole pair (ehp) under UV or visible irradiation (Huang et al., 2015; Le et al., 2019). The electron and hole combine with the adsorbed oxygen ($O^{\cdot}$) on the photocatalyst surface and water (H_2O) to generate O_2 and hydroxyl (OH), which help in the oxidation of organic products into end products (CO_2 and H_2O) (Senapati et al., 2012). Photocatalysis has been regarded as a significant approach for pollutant removal due to its high sustainability, improved efficiency, and low energy consumption (Shen et al., 2021a; Li et al., 2022b) The investigation of photocatalysts with remarkable features such as extraordinary sunlight absorption, significant generation, and separation of charge carriers with enhanced redox potential is quite useful for achieving efficient photocatalytic removal of pollutant (Idrees et al., 2016; Li et al., 2022c). Photocatalysts, a green technology that uses solar energy, have a significant impact on environmental restoration. Therefore, more time is required to investigate potential photocatalysts (Li et al., 2022a; Cai et al., 2022; Li et al., 2022d). In this aspect, lead tri-halide with unique properties could also be used in the photochemical conversion, if the issues of stability, inefficient photocatalytic activity, and rigorous ehp recombination rate could be optimized (Zhao et al., 2020). There have recently been a few reports on the use of inorganic lead tri-halide perovskites, their derivatives, and composites as photocatalysts. Among the cesium-based lead halides, it was observed that pristine bromide-based compounds with a wide-bandgap are difficult to photocatalyze; however, after different treatments such as making a heterostructure or changing the typical ligands are an optimal choice (Xu et al., 2017). Moreover, photoreduction of CO_2 and hydrogen evolution using a mixture of Br/Cl and Br/I has been reported (Guan et al., 2019). In comparison to these inorganic halides, cesium lead iodide ($CsPbI_3$) had a narrow bandgap of 1.73 eV, high emission intensity, and existed in two major phases known as alpha phase (α-$CsPbI_3$) and delta phase (δ-$CsPbI_3$) (Lai et al., 2017). Lin et al., recently reported the use of $CsPbI_3$ as a photocatalyst by making heterostructure with tungsten disulfide (WS_2), where they used γ-$CsPbI_3$ nanocrystals fabricated with several layered tungsten disulfides for the complete degradation of methylene blue (MB) into less toxic inorganic products with high photocatalytic degradation efficiency (Zhang et al., 2019). The coupling of inorganic perovskites with other compounds is considered as useful strategy for addressing the issues of instability, photocatalytic activity deficiency, and controlled ehp recombination. Ma et al. reported on the photocatalytic activity of graphitic carbon nitride (g-C_3N_4) combined with $CsPbI_3$ for photocatalytic degradation of the organic dye rhodamine B, and they also reported the use of Pt as a co-catalyst for hydrogen generation by water splitting (Liu and Ma, 2021). Up to now, there are no reports about the photocatalytic degradation of inorganic pollutants from water streams by the $CsPbX_3$/ZnO heterostructure.

Here, for the first time, we used $CsPbX_3$/ZnO heterostructure with ZnO as a photocatalyst to study the photocatalytic activity of $CsPbX_3$. (Zhang et al., 2021a). Although Xu et al., recently reported a $CsPbX_3$/ZnO heterostructure for light-emitting diodes. Wang et al., also used ZnO as a basis for transporting electrons to solar cells (Deng et al., 2020). To date, however, no reports have been found regarding the use of ZnO and $CsPbX_3$ for photocatalytic applications. This study is aimed at modifying $CsPbI_3$, and $CsPbBr_3$ using ZnO with the desired properties for the efficient photo degradation of heavy metals. We investigated the photocatalytic response in $CsPbI_3$, $CsPbBr_3$ forming heterostructures with ZnO and the results proved that δ-$CsPbI_3$/ZnO heterostructure is quite beneficial in the photo degradation of heavy metals under visible light with an efficiency of more than 50%, owing to its hexagonal structure.

2 Materials and method

2.1 Materials

Cesium carbonate (Cs_2CO_3, 99.99%) was bought from Macklin. Lead iodide (PbI_2, 99.99%), Lead bromide ($PbBr_2$, 99.99%), Octadecene (ODE, technical grade 90%), Oleic acid (OA, technical grade 90%), oleylamine (OAm, technical grade 70%), Zinc Stearate ($ZnSt_2$, 98%), Toluene (98%) and Hexane (99.9%) were purchased from Sigma Aldrich and used as it is received without any further modification.

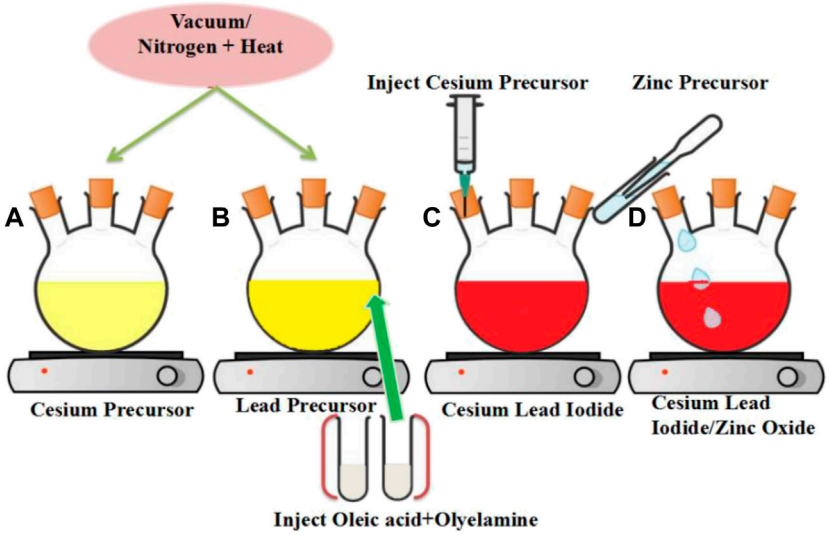

FIGURE 1
Schematic representation for the synthesis of the $CsPbI_3$/ZnO heterostructure **(A)** Cesium precursor **(B)** Lead precursor **(C)** formation of Cesium Lead Iodide **(D)** formation of Cesium Lead Iodide/Zinc Oxide heterostructure.

2.2 Photocatalysts synthesis

2.2.1 Formation of cesium and lead halide precursors by hot injection method

Protesescu's hot injection strategy was used for the synthesis of $CsPbX_3$/ZnO heterostructure, with minor modifications (Protesescu et al., 2015). The stepwise schematic presentation is shown in Figure 1. Firstly, 0.6 g of cesium carbonate (Cs_2CO_3), 2 ml OA, and 20 ml ODE were added to a 50 ml 3-neck round bottom flask and stirred continuously under vacuum for 30 min at 125°C, absolving the flask with nitrogen (N_2) for 10 min, it was placed back under vacuum. An alternative implication of vacuum and N_2 to completely remove moisture and oxygen has been applied as shown in Figure 1A. The PbI_2/Br_2 precursors were then synthesized by degassing 0.8 g of PbI_2 and 0.6 g of $PbBr_2$ in 20 ml ODE for 1 h under constant stirring and heating at 125°C in a 50 ml flask. The flask was then filled with a 1:1 mixture of OA and OAm (4 ml each, pre-heated at ~70°C) and vacuumed again for 15–30 min, until the salt of lead halides was completely dissolved and the solution was no longer releasing gas (15–30 min), as shown in Figure 1B.

2.3 Formation of cesium lead halide/zinc oxide heterostructure

For the formation of cesium lead halides, the temperature of the lead halide precursor was raised to 150°C, and 4 ml cesium precursor was injected swiftly under a nitrogen environment, as shown in Figure 1C. Later, for the photocatalytic activity investigation of as synthesized $CsPbX_3$ with Zinc oxide, 0.4 mg ml^{-1} zinc stearate in ODE was injected into the above mixture as a zinc source for the formation of $CsPbX_3$/ZnO heterostructure as shown in Figure 1D, aliquotes were taken at different times, and the reaction was quenched by dipping the flask into the ice bath. Finally, the solution was centrifuged for 3 min at 10,000 rpm, the supernatant was discarded, and precipitates were dispersed in toluene/hexane for further investigation.

2.4 Characterization techniques

X-ray diffraction patterns (XRD) spectra was collected X-ray diffractometer (Bruker D8 advance, Germany) with Cu K_α radiation (k = 1.54 nm) in the range of 2θ = 20°–70°. The valence properties of all existing elements in $CsPbX_3$/ZnO NPs were determined by employing X-ray photoelectron (XPS: ESCALAB 250Xi-system) Ultraviolet-visible (UV-visible) spectra were investigated by a Lambda 950 spectrophotometer in the wavelength range of 300–800 nm. Fourier Transform Infrared (FTIR) has been carried out by Shimadzu-8400S infrared spectrometer. The morphology of the material was investigated by transmission electron microscope (JEOL JSM-7800F) and energy-dispersive spectra (EDS) was obtained by using an integrated Oxford INCA X-ACT equipped with SEM. On a multi-channel battery system (LANHE-CT2001A), the electrocatalytic activity of prototype coin cells was studied in a voltage range of 0.1–3.0 V at a constant current density.

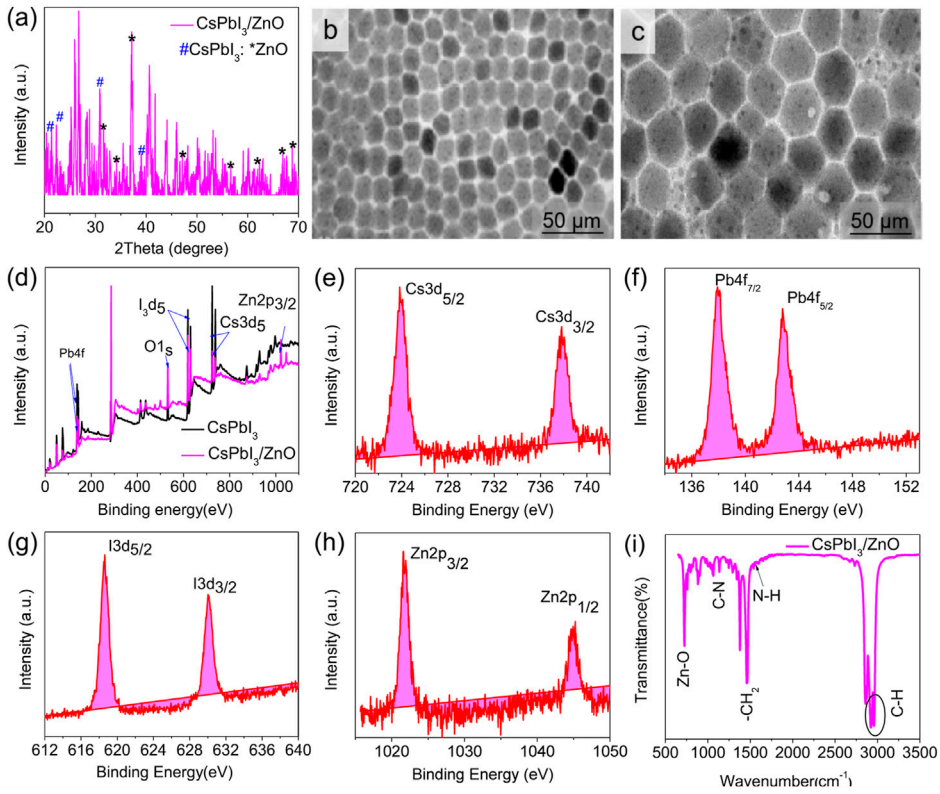

FIGURE 2
(A) X-ray diffraction (XRD) pattern of $CsPbI_3$/ZnO heterostructure, **(B,C)** TEM images of $CsPbI_3$ and $CsPbI_3$/ZnO heterostructure. **(D)** The general XPS spectrum and **(E–H)** HR-XPS spectrum of $CsPbI_3$/ZnO heterostructure. **(I)** FTIR spectra of $CsPbI_3$/ZnO heterostructure.

2.5 Photocatalytic activity measuring experiment

The photocatalytic activity of $CsPbX_3$/ZnO heterostrucutre as a photocatalyst was irradiated to a 300W xenon lamp in ambient conditions. For which ZnO (0.4 $mgmL^{-1}$ $ZnSt_2$ in ODE) was injected to $CsPbX_3$ solution, under constant magnetic stirring and heating to achieve equilibrium. For the photocatalytic inquiry, two different temperatures have been used i.e., 100°C and 160°C. After injecting zinc precursor into the halide perovskites, samples were prepared using 15 μL ($CsPbX_3$/ZnO) in 1 ml hexane at different time intervals starting from 2 min till 30min. Photocatalytic activity under UV-visible spectrophotometer in the wavelength range of 300–800 nm has been observed. To explore the photocatalytic activity of ZnO as a photocatalyst, the absorbance spectra of halide perovskites with and without zinc oxide were compared.

Degradation efficiency (%) has been calculated by using Eq. 1.

$$\text{Degradation } (\%) = [(C_o - C_t)/C_o]*100, \quad (1)$$

where C_o is degradation concentration without ZnO and C_t degradation concentration with ZnO at different intervals in the above relation (Huang et al., 2015; Sajid et al., 2020).

3 Results and discussions

3.1 Characterization of $CsPbX_3$/ZnO heterostructure

Studies have shown that inorganic cesium lead halide perovskite is considered as a hot area for scientists and researchers due to its outstanding performance in different applications. Different reports highlight its usage as photocatalysts for CO_2 reduction (Wang et al., 2019), hydrogen evolution (Zhao et al., 2021) and degradation of different pollutants from the environment and industry (Zhao et al., 2020; Li et al., 2023). To investigate the as-synthesized system of $CsPbX_3$/ZnO heterostructure, different investigations have been carried out. Figure 2A is the XRD pattern of the $CsPbI_3$/ZnO heterostructure. The XRD pattern confirmed the presence of both $CsPbI_3$ and ZnO, which are highlighted with

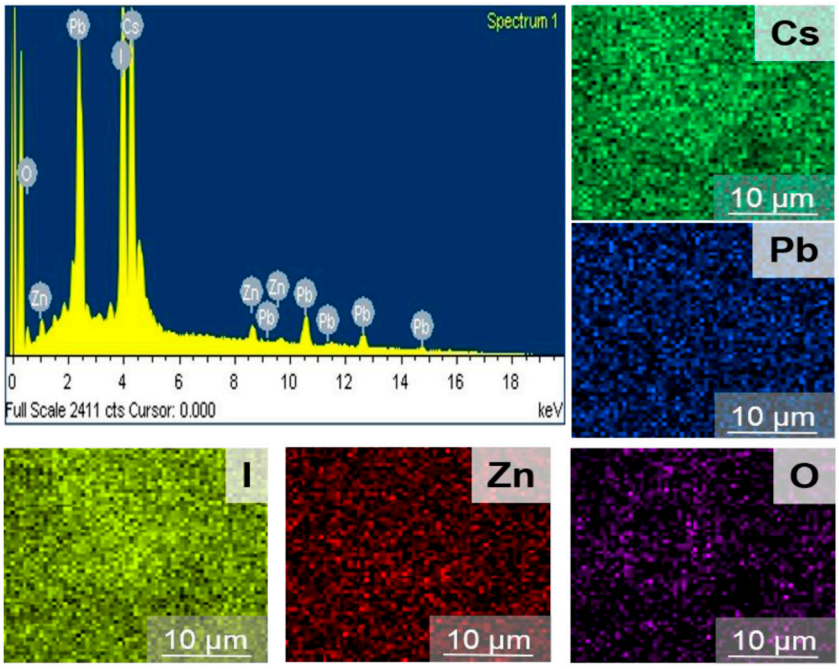

FIGURE 3
EDS spectra of $CsPbI_3$/ZnO heterostructure and its corresponding elements' EDS mapping.

different symbols. All of the characteristic peaks correspond to JCPDS card number. 18–0376 and 36–1,451, which represent the delta and wurtzite phases, respectively. The diffraction peaks located at 21.6°, 22.7°,31.3°, and 39.3° indicate the presence of $CsPbI_3$ (highlighted with #), whereas the peaks at 31.8°,34.4°, 36.2°, 47.5°, 56.5°, 62.8°, 66.3°, and 67.9° correspond to the ZnO (represented with *) (Zhang et al., 2007). Figures 2B,C show the morphology of $CsPbI_3$ and $CsPbI_3$/ZnO heterostructures having the hexagonal geometry of $CsPbI_3$ with an average particle size of 28.3 nm that has been enlarged to 34.5 nm after the addition of photocatalyst ZnO, proving the inclusion of ZnO with the retention of the same hexagonal morphology. The dots on the surface of Figure 2C justifying the formation of the $CsPbI_3$/ZnO heterostructure.

XPS analysis was conducted to investigate the chemical states of elements presented in the as-synthesized $CsPbI_3$/ZnO heterostructure (Figure 2D). The general XPS survey spectrum proves the existence of Cs, Pb, I, Zn, and O, confirming the formation of $CsPbI_3$/ZnO. Figures 2E–H presents the HR-XPS deconvoluted peaks of all existing elements.

The HR-XPS Cs spectrum deconvoluted into peaks at 723.86 and 737.83 eV, ascribed to the Cs3d of $Cs3d_{5/2}$ and $Cs3d_{3/2}$, respectively (Figure 2E). The peaks at 137.96 and 142.80 eV in the core level spectrum of Pb4f are attributed to $Pb4f_{7/2}$ and $Pb4f_{5/2}$, respectively (Figure 2F). Similarly, the core-level I3d spectrum position at 618.61 eV indicated the presence of $I3d_{5/2}$ and 630 eV $I3d_{3/2}$ (Figure 2G), while the peaks at 1,021.9 and 1,044.94 eV were attributed to the formation of $Zn2p_{3/2}$ and $Zn2p_{1/2}$ (Zn-O), respectively (Figure 2H) (Lu et al., 2018; Pirhashemi et al., 2019).

TABLE 1 Elemental percentage of as-synthesized $CsPbI_3$/ZnO heterostructure.

Elements	Atomic percentages (%)
Cs	16.78
Pb	14.40
I	55.02
Zn	6.27
O	7.53

The surface functionality of the materials was recorded by FTIR spectrum in the range of 650–3,500 cm^{-1}. Figure 2I shows the FTIR spectra of the $CsPbI_3$/ZnO heterostructure in which the peak at 716 cm^{-1} shows the bonding between Zn-O, whereas the rest of the peaks show the presence of different ligands used for the formation of heterostructure. Generally, the peak at 1,153 cm^{-1} represents C-N, 1,473 cm^{-1} shows -CH_2, 1,641 cm^{-1} to N-H, and 2,913 and 2,955 cm^{-1} correspond to the presence of C-H attributed due to the aliphatic chains of octadecyl, oleylamine and oleic acid (An et al., 2018) (Nipane et al., 2013). EDS was used to investigate the elemental percentages in the synthesized compound, as shown in Figure 3.

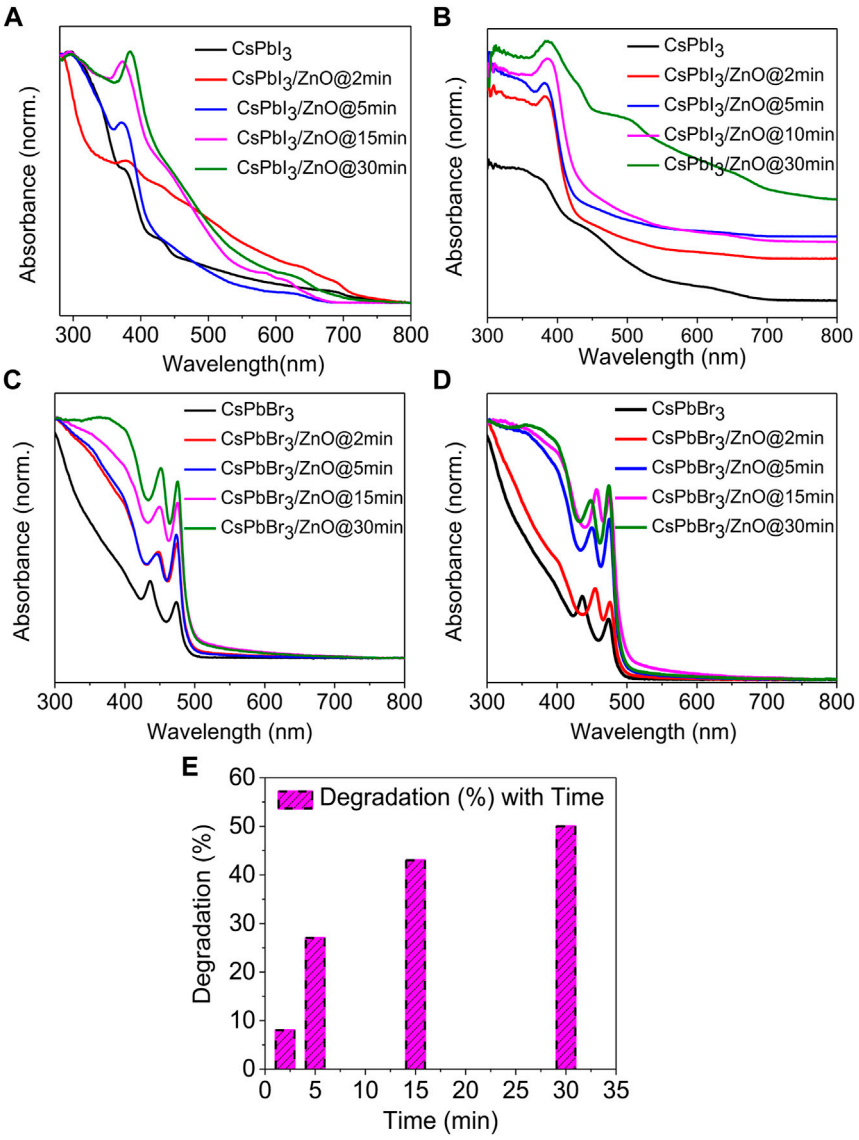

FIGURE 4
UV-visible absorbance spectra of $CsPbI_3$ and $CsPbI_3$/ZnO as a function of time at **(A)** 100°C and **(B)** 160°C. $CsPbBr_3$ and $CsPbBr_3$/ZnO at **(C)** 100°C and **(D)** 160°C. **(E)** Degradation efficiency with time for $CsPbI_3$/ZnO heterostructure.

The EDS spectrum confirms the existence and equal distribution of all the elements in the synthesized compound, and their atomic percentage is listed in Table 1.

3.2 Photocatalytic activity of $CsPbX_3$/ZnO heterostructure

The basic photocatalytic mechanism starts with the generation of electrons and holes generated as a result of light irradiation with a wavelength greater than or equal to their bandgap; photo-induced electrons move from the valence band (VB) to the conduction band (CB), and corresponding holes move to the valence band. Hence, a redox reaction was carried out using these isolated electron-hole pairs (Ren et al., 2022). The as-synthesized product was optically characterized using UV-visible spectroscopy to analyze the behavior of inorganic halide perovskites with ZnO as a photocatalyst. The designed composite heterostructure is made up of interfaces made of various materials that are tightly bonded and have indistinguishable interface junctions (Zhao et al., 2018). The benefit of using zinc is that it has the capability to replace lead during the formation of heterostructure,

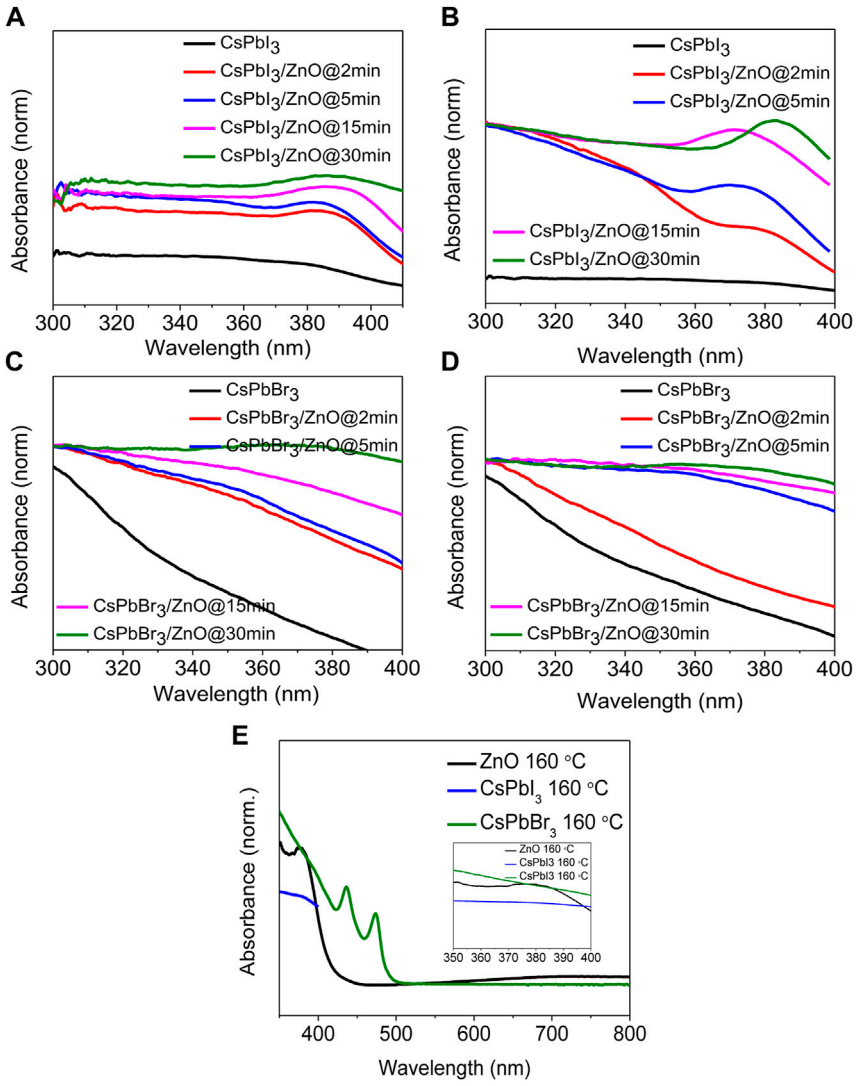

FIGURE 5
Absorbance spectra of inorganic $CsPbI_3$ and $CsPbI_3$/ZnO heterostructures at **(A)** 100°C and **(B)** 160 C. Absorbance spectra of inorganic $CsPbBr_3$ and $CsPbBr_3$/ZnO heterostructures at **(C)** 100 C and **(D)** 160 C. **(E)** Absorbance spectra for the controlled samples of $CsPbI_3$ and ZnO. Inset shows the close view.

indicating the potential to be used as a heavy metal degradation and water pollution removal catalyst (Kar et al., 2022).

The UV-visible absorption spectra of two different inorganic lead halide perovskite ($CsPbI_3$ and $CsPbBr_3$) with ZnO as a photocatalyst for two temperatures, low (100°C) and high (160°C), with activity times ranging from 2 to 30 min, as shown in Figures 4A–D. Figures 4A,B shows that $CsPbI_3$ possesses the highest photocatalytic activity, whereas Figures 4C,D represents that $CsPbBr_3$ has no effect on ZnO even at elevated temperatures. It was observed that pristine $CsPbBr_3$ has negligible photocatalytic activity due to obvious surface defects that introduce shallow transition levels and act as charge recombination sites, and also the material's wider bandgap, which limits its use as a photocatalytic material. In comparison to $CsPbBr_3$, $CsPbI_3$ has a narrow bandgap of 1.73 eV and higher emission intensity, exhibiting the potential for excessive photo-generated ehp for photocatalysis (Tang et al., 2019; Zhang et al., 2019; Wang et al., 2021). ZnO's good electron mobility, high absorption tendency, and cost-effectiveness make it an ideal photocatalyst. Coupling ZnO with halide perovskites enhances the generation of ehp by reducing the formation energy of the perovskites (Senapati et al., 2012; Jiang et al., 2019; Deng et al., 2020). Figures 4A,B show an absorbance peak from 370–385 nm due to zinc adsorption, confirming the presence of ZnO (Das et al., 2020; Karami et al., 2020), whereas, in Figures

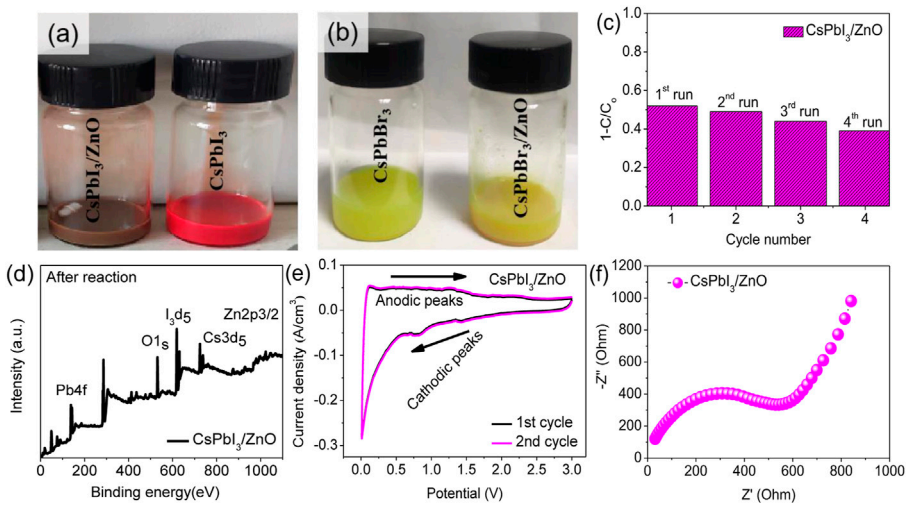

FIGURE 6
Adsorption of **(A)** $CsPbI_3$/ZnO and $CsPbI_3$, and **(B)** $CsPbBr_3$/ZnO and $CsPbBr_3$ heterostructure. **(C)** Cyclic stability of $CsPbI_3$/ZnO under UV light. **(D)** Post-XPS analysis of $CsPbI_3$/ZnO **(E)** Cyclic voltammograms of $CsPbI_3$/ZnO at a scanning rate of 0.1 mV s^{-1} and **(F)** Nyquist plot at room temperature for $CsPbI_3$/ZnO heterostructure.

4C,D show no change in the spectra, indicating that there is no zinc adsorption. Figures 5A,B depicts the obvious zinc adsorption in the $CsPbI_3$/ZnO heterostructure by depicting the obvious absorbance peaks from 370–385 nm at both temperatures as compared to controlled samples of $CsPbI_3$ and ZnO (Figure 5E), while Figures 5C,D represent no discernible change in the spectra. So, here we calculated the degradation efficiency with time in synthesized samples of $CsPbI_3$/ZnO heterostructure at high temperature yielding a degradation efficiency of 52% by using Eq. 1 shown in Figure 4E.

The cycling stability of a photocatalyst is important for practical usage. Therefore, recycling experiments are carried out for $CsPbI_3$/ZnO. The results are shown in Figure 5C suggested that the catalyst's performance is negligible after four continuous cycles of photocatalyst reutilization. This study confirms that $CsPbI_3$/ZnO is highly stable to heavy metal phtodegradation. The post-xps analysis indicted that the peaks for all the core elements are greatly reduced with decreasing intensity, confirming the photodegradation of heavy metals (d).

3.3 Cyclic voltammograms and AC impedance analysis of the $CsPbI_3$/ZnO heterostructure

The electrochemical performance of $CsPbI_3$/ZnO was assessed to confirm its potential as a photocatalyst. In Figure 6E, the oxidative and reductive properties of the $CsPbI_3$/ZnO heterostructure were investigated using the characteristic cyclic voltammogram test at a scanning rate of 0.1 mV s^{-1}. The CV curve for the first cycle presented characteristic discharge peaks at 0.82 and 1.41 V, which are the reduction peaks that confirm the successful reaction of $CsPbI_3$/ZnO heterostructure. Moreover, cathodic peaks confirm electrolyte decomposition and the formation of an SEI passivation layer on the surface of anode material during discharge. Two oxidative peaks were observed in the anodic sweep at 1.25 V, corresponding to a gradual Zn^+ withdrawal process in $CsPbI_3$/ZnO. The CV test confirms the oxidation and reduction potentials of $CsPbI_3$/ZnO heterostructure. The electrochemical impedance spectra with a wide-range of frequency as shown in Figure 6F. The Nyquist curve consists of a semicircle and an oblique line from high to medium-frequency and high to low-frequency regions, respectively. The semicircle in the high-frequency region defined the extent of resistance to electron transfer, confirming the negligible ion transformation and bulk polarization, while the straight line represents the high electrical conductivity of the $CsPbI_3$/ZnO catalyst. The result showed that the $CsPbI_3$/ZnO catalyst had high electrical conductivity and was conductive to zinc ion diffusion.

3.4 Photocatalytic mechanism

Figure 7 depicts the photocatalytic mechanism of $CsPbX_3$/ZnO heterostructure. Generally, the photocatalytic process initiates with the generation of electron hole pairs (ehp) in

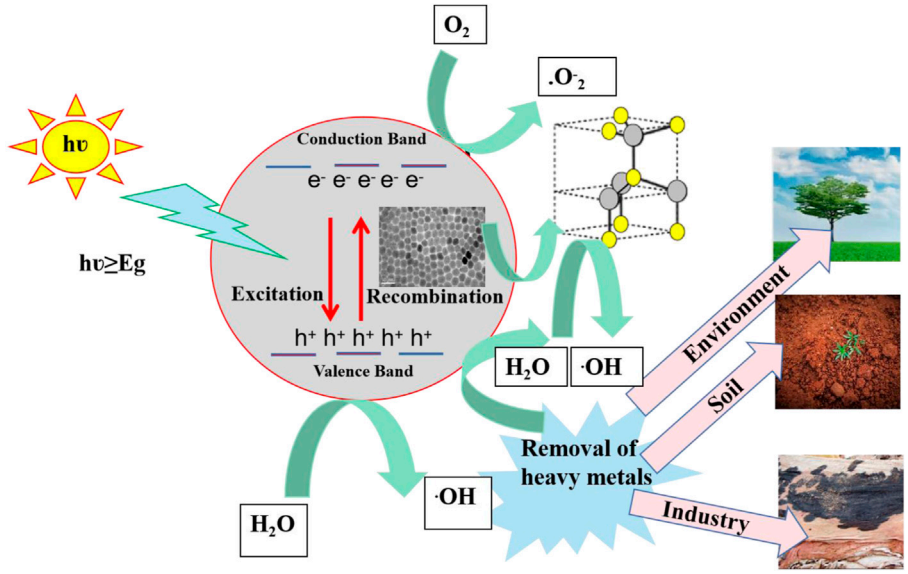

FIGURE 7
Schematic representation of the photocatalytic mechanism of $CsPbX_3$/ZnO heterostructure.

the presence of light with an energy greater than or equal to the bandgap (Wang et al., 2022). The electrons from the valence band (VB) are excited towards the conduction band (CB) of perovskites, thereby generating photo-active species including e^- and h^+. Such photogenerated e^- would either combine with the h^+ or be arbitrarily shifted to the surface of the photocatalysts, further trapped by O_2 to generate $O_2^{\cdot-}$.for the further generation of . OH (Wei et al., 2021). The formation of heterostructure has been regarded as an effective strategy for the retardation of the e/h recombination by keeping the utmost redox potential of a photocatalyst (Shen et al., 2022). Particularly, in this case of perovskite heterostructure, the generation of ehp occurs on the surface of $CsPbX_3$ when an electron (e^-) in the $CsPbX_3$/ZnO shifts (excites) from the valence band (VB, HOMO) to the conduction band (CB, LUMO) and leaves holes (h^+) in the HOMO region, known as the generation of ehp. In the $CsPbX_3$ perovskite, these as-produced ehp react with H_2O and O_2, generating excessive hydroxyl radicals (·OH) and oxygen molecules (O_2^-) (Zhang et al., 2019). After the introduction of ZnO, holes can be shifted from the halide perovskite to the surface of ZnO, generating (·OH). The overall mechanism can be summarized as follows:

$$CsPbX_3 + h \rightarrow e^- + h^+, \quad (2)$$

$$O_2 + e^- \rightarrow .O_2^-, \quad (3)$$

$$H_2O + h^+ \rightarrow .OH + H^+, \quad (4)$$

$$ZnO + H^+ \rightarrow Zn^+ + \cdot OH \quad (5)$$

Thus, the produced radicals help in the reduction of heavy metals into environment-friendly end products like CO_2 and H_2O (Das et al., 2020; Khan and Pathak, 2020). Hence, these synthesized $CsPbX_3$/ZnO heterostructures are quite useful in removing heavy metals and toxic products from the environment, soil, and different industry.

4 Conclusion

In conclusion, we have successfully synthesized the $CsPbX_3$/ZnO heterostructure with zinc oxide as a photocatalyst using a standard hot injection method. The as-synthesized material was characterized by using different structural characterizations to confirm the successful formation and its morphological structure. The $CsPbI_3$/ZnO heterostructure exhibits a degradation efficiency of 52%, which is higher than the degradation efficiency of $CsPbI_3$ with various other dyes. The CV and EIS analysis show high oxidation and reduction characteristics, as well as superior resistance to electron transfer, confirming the electrical conductivity. Thus, this synthesized heterostructure has the potential to be used for heavy metal degradation as well as a water cleaning catalyst.

Data availability statement

The original contributions presented in the study are included in the article/Supplementary Material, further inquiries can be directed to the corresponding author.

Author contributions

SG: Conception and design of the study, drafting of the manuscript, Acquisition of data SB: Conception and design of study, Review and edit manuscript GL: Review and editing, Supervision. MI: Review and edit manuscript.

Acknowledgments

The authors would like to acknowledge the postdoctoral research fellowship program of Shenzhen University and appreciate the technical support at the University for assistance in using the equipment.

Conflict of interest

The authors declare that the research was conducted in the absence of any commercial or financial relationships that could be construed as a potential conflict of interest.

Publisher's note

All claims expressed in this article are solely those of the authors and do not necessarily represent those of their affiliated organizations, or those of the publisher, the editors and the reviewers. Any product that may be evaluated in this article, or claim that may be made by its manufacturer, is not guaranteed or endorsed by the publisher.

References

Akkerman, Q. A., D'innocenzo, V., Accornero, S., Scarpellini, A., Petrozza, A., Prato, M., et al. (2015). Tuning the optical properties of cesium lead halide perovskite, 137, 10276–10281.*Nanocrystals by anion exchange reactionsJ. Am. Chem. Soc*,

An, R., Zhang, F., Zou, X., Tang, Y., Liang, M., Oshchapovskyy, I., et al. (2018). Photostability and photodegradation processes in colloidal $CsPbI_3$ perovskite quantum dots. *ACS Appl. Mat. Interfaces* 10, 39222–39227. doi:10.1021/acsami.8b14480

Batool, S., Idrees, M., Javed, M. S., Saleem, M., and Kong, J. (2020). Engaging tailored capacity of layered WS_2 via sulphur bonding coupled with polyetherimide (WS_2@NC) nanocomposite for high power and improved lithium-ion storage. *Mater. Chem. Phys.* 246, 122832. doi:10.1016/j.matchemphys.2020.122832

Cai, M., Wang, C., Liu, Y., Yan, R., and Li, S. (2022). Boosted photocatalytic antibiotic degradation performance of $Cd_{0.5}Zn_{0.5}S$/carbon dots/Bi_2WO_6 S-scheme heterojunction with carbon dots as the electron bridge. *Sep. Purif. Technol.* 300, 121892. doi:10.1016/j.seppur.2022.121892

Cheng, L., Xiang, Q., Liao, Y., and Zhang, H. (2018). CdS-based photocatalysts. *Energy Environ. Sci.* 11, 1362–1391. doi:10.1039/c7ee03640j

Das, S., Paul, T., Maiti, S., and Chattopadhyay, K. K. (2020). Ambient processed $CsPbX_3$ perovskite cubes for photocatalysis. *Mater. Lett.* 267, 127501. doi:10.1016/j.matlet.2020.127501

Deng, W., Li, J., Jin, J., Mishra, D. D., Xin, J., Lin, L., et al. (2020). Fast and low temperature processed $CsPbI_3$ perovskite solar cells with ZnO as electron transport layer. *J. Power Sources* 480, 229134. doi:10.1016/j.jpowsour.2020.229134

Fujishima, A., Rao, T. N., and Tryk, D. A. (2000). Titanium dioxide photocatalysis. *J. Photochem. Photobiol. C Photochem. Rev.* 1, 1–21. doi:10.1016/s1389-5567(00)00002-2

Guan, Z., Wu, Y., Wang, P., Zhang, Q., Wang, Z., Zheng, Z., et al. (2019). Perovskite photocatalyst $CsPbBr_{3-x}I_x$ with a bandgap funnel structure for H_2 evolution under visible light. *Appl. Catal. B Environ.* 245, 522–527. doi:10.1016/j.apcatb.2019.01.019

Gull, S., Yang, Z., Wu, W., Rao, Q., Zhang, J., and Li, W. (2020). Multi-phased cesium lead iodide quantum dots with large Stokes shift. *Mater. Lett.* 271, 127765. doi:10.1016/j.matlet.2020.127765

Hitam, C., and Jalil, A. (2020). A review on exploration of Fe_2O_3 photocatalyst towards degradation of dyes and organic contaminants. *J. Environ. Manag.* 258, 110050. doi:10.1016/j.jenvman.2019.110050

Huang, N., Shu, J., Wang, Z., Chen, M., Ren, C., and Zhang, W. (2015). One-step pyrolytic synthesis of ZnO nanorods with enhanced photocatalytic activity and high photostability under visible light and UV light irradiation. *J. Alloys Compd.* 648, 919–929. doi:10.1016/j.jallcom.2015.07.039

Idrees, M., Batool, S., Hussain, Q., Ullah, H., Al-Wabel, M. I., Ahmad, M., et al. (2016). High-efficiency remediation of cadmium (Cd^{2+}) from aqueous solution using poultry manure-and farmyard manure-derived biochars. *Sep. Sci. Technol.* 51, 2307–2317. doi:10.1080/01496395.2016.1205093

Jiang, Y., Liao, J.-F., Xu, Y.-F., Chen, H.-Y., Wang, X.-D., and Kuang, D.-B. (2019). Hierarchical $CsPbBr_3$ nanocrystal-decorated ZnO nanowire/macroporous graphene hybrids for enhancing charge separation and photocatalytic CO_2 reduction. *J. Mat. Chem. A Mat.* 7, 13762–13769. doi:10.1039/c9ta03478a

Johar, M. A., Afzal, R. A., Alazba, A. A., and Manzoor, U. (2015). Photocatalysis and bandgap engineering using ZnO nanocomposites. *Adv. Mater. Sci. Eng.*, 1–22. 2015, doi:10.1155/2015/934587

Kar, M., Chakraborty, R., Patel, U., Ray, S., Acharya, T., Goswami, C., et al. (2022). Impact of Zn-doping on the composition, stability, luminescence properties of silica coated all-inorganic cesium lead bromide nanocrystals and their biocompatibility. *Mater. Today Chem.* 23, 100753. doi:10.1016/j.mtchem.2021.100753

Karami, M., Ghanbari, M., Amiri, O., and Salavati-Niasari, M. (2020). Enhanced antibacterial activity and photocatalytic degradation of organic dyes under visible light using cesium lead iodide perovskite nanostructures prepared by hydrothermal method. *Sep. Purif. Technol.* 253, 117526. doi:10.1016/j.seppur.2020.117526

Khan, S. H., and Pathak, B. (2020). Zinc oxide based photocatalytic degradation of persistent pesticides: A comprehensive review. *Environ. Nanotechnol. Monit. Manag.* 13, 100290. doi:10.1016/j.enmm.2020.100290

Kulkarni, S. A., Mhaisalkar, S. G., Mathews, N., and Boix, P. P. (2019). Perovskite nanoparticles: Synthesis, properties, and novel applications in photovoltaics and LEDs. *Small Methods* 3, 1800231. doi:10.1002/smtd.201800231

Lai, M., Kong, Q., Bischak, C. G., Yu, Y., Dou, L., Eaton, S. W., et al. (2017). Structural, optical, and electrical properties of phase-controlled cesium lead iodide nanowires. *Nano Res.* 10, 1107–1114. doi:10.1007/s12274-016-1415-0

Le, A. T., Pung, S.-Y., Sreekantan, S., Matsuda, A., and Huynh, D. P. (2019). Mechanisms of removal of heavy metal ions by ZnO particles. *Heliyon* 5, e01440. doi:10.1016/j.heliyon.2019.e01440

Lee, G.-J., and Wu, J. J. (2017). Recent developments in ZnS photocatalysts from synthesis to photocatalytic applications—a review. *Powder Technol.* 318, 8–22. doi:10.1016/j.powtec.2017.05.022

Li, S., Cai, M., Liu, Y., Zhang, J., Wang, C., Zang, S., et al. (2022a). *In situ* construction of a C_3N_5 nanosheet/Bi_2WO_6 nanodot S-scheme heterojunction with enhanced structural defects for the efficient photocatalytic removal of tetracycline and Cr(vi). *Inorg. Chem. Front.* 9, 2479–2497. doi:10.1039/d2qi00317a

Li, S., Cai, M., Wang, C., Liu, Y., Li, N., Zhang, P., et al. (2022b). Rationally designed Ta_3N_5/BiOCl S-scheme heterojunction with oxygen vacancies for elimination of tetracycline antibiotic and Cr(VI): Performance, toxicity evaluation and mechanism insight. *J. Mater. Sci. Technol.* 123, 177–190. doi:10.1016/j.jmst.2022.02.012

Li, S., Wang, C., Cai, M., Liu, Y., Dong, K., and Zhang, J. (2022c). Designing oxygen vacancy mediated bismuth molybdate (Bi_2MoO_6)/*N*-rich carbon nitride (C_3N_5) S-scheme heterojunctions for boosted photocatalytic removal of tetracycline antibiotic and Cr(VI): Intermediate toxicity and mechanism insight. *J. Colloid Interface Sci.* 624, 219–232. doi:10.1016/j.jcis.2022.05.151

Li, S., Wang, C., Cai, M., Yang, F., Liu, Y., Chen, J., et al. (2022d). Facile fabrication of TaON/Bi_2MoO_6 core-shell S-scheme heterojunction nanofibers for boosting visible-light catalytic levofloxacin degradation and Cr(VI) reduction. *Chem. Eng. J.* 428, 131158. doi:10.1016/j.cej.2021.131158

Li, S., Cai, M., Liu, Y., Wang, C., Yan, R., and Chen, X. (2023). Constructing $Cd_{0.5}Zn_{0.5}S$/Bi2WO_6 S-scheme heterojunction for boosted photocatalytic antibiotic oxidation and Cr(VI) reduction. *Adv. Powder Mater.* 2, 100073. doi:10.1016/j.apmate.2022.100073

Liu, Y., and Ma, Z. (2021). Combining g-C3N4 with CsPbI3 for efficient photocatalysis under visible light. *Colloids Surfaces A Physicochem. Eng. Aspects* 628, 127310. doi:10.1016/j.colsurfa.2021.127310

Lu, C., Li, H., Kolodziejski, K., Dun, C., Huang, W., Carroll, D., et al. (2018). Enhanced stabilization of inorganic cesium lead triiodide ($CsPbI_3$) perovskite quantum dots with tri-octylphosphine. *Nano Res.* 11, 762–768. doi:10.1007/s12274-017-1685-1

Nipane, D., Thakare, S., and Khati, N. (2013). Synthesis of novel ZnO having cauliflower morphology for photocatalytic degradation study. *J. Catal.*, 1–8. 2013, doi:10.1155/2013/940345

Pirhashemi, M., Elhag, S., Adam, R. E., Habibi-Yangjeh, A., Liu, X., Willander, M., et al. (2019). n–n ZnO–Ag_2CrO_4 heterojunction photoelectrodes with enhanced visible-light photoelectrochemical properties. *RSC Adv.* 9, 7992–8001. doi:10.1039/c9ra00639g

Protesescu, L., Yakunin, S., Bodnarchuk, M. I., Krieg, F., Caputo, R., Hendon, C. H., et al. (2015). Nanocrystals of cesium lead halide perovskites ($CsPbX_3$, X= Cl, Br, and I): Novel optoelectronic materials showing bright emission with wide color gamut. *Nano Lett.* 15, 3692–3696. doi:10.1021/nl5048779

Ren, K., Yue, S., Li, C., Fang, Z., Gasem, K. A., Leszczynski, J., et al. (2022). Metal halide perovskites for photocatalysis applications. *J. Mat. Chem. A Mat.* 10, 407–429. doi:10.1039/d1ta09148d

Sajid, M. M., Shad, N. A., Javed, Y., Khan, S. B., Zhang, Z., Amin, N., et al. (2020). Preparation and characterization of Vanadium pentoxide (V_2O_5) for photocatalytic degradation of monoazo and diazo dyes. *Surfaces Interfaces* 19, 100502. doi:10.1016/j.surfin.2020.100502

Senapati, S., Srivastava, S. K., and Singh, S. B. (2012). Synthesis, characterization and photocatalytic activity of magnetically separable hexagonal Ni/ZnO nanostructure. *Nanoscale* 4, 6604–6612. doi:10.1039/c2nr31831h

Shen, X., Yang, J., Zheng, T., Wang, Q., Zhuang, H., Zheng, R., et al. (2020). Plasmonic pn heterojunction of Ag/Ag_2S/Ag_2MoO_4 with enhanced Vis-NIR photocatalytic activity for purifying wastewater. *Sep. Purif. Technol.* 251, 117347. doi:10.1016/j.seppur.2020.117347

Shen, X., Yang, Y., Song, B., Chen, F., Xue, Q., Shan, S., et al. (2021a). Magnetically recyclable and remarkably efficient visible-light-driven photocatalytic hexavalent chromium removal based on plasmonic biochar/bismuth/ferroferric oxide heterojunction. *J. Colloid Interface Sci.* 590, 424–435. doi:10.1016/j.jcis.2021.01.095

Shen, X., Zhang, Y., Shi, Z., Shan, S., Liu, J., and Zhang, L. (2021b). Construction of C_3N_4/CdS nanojunctions on carbon fiber cloth as a filter-membrane-shaped photocatalyst for degrading flowing wastewater. *J. Alloys Compd.* 851, 156743. doi:10.1016/j.jallcom.2020.156743

Shen, X., Song, B., Shen, X., Shen, C., Shan, S., Xue, Q., et al. (2022). Rationally designed S-scheme heterojunction of C_3N_4/Bi_2MoO_6/carbon fiber cloth as a recyclable, macroscopic and efficient photocatalyst for wastewater treatment. *Chem. Eng. J.* 445, 136703. doi:10.1016/j.cej.2022.136703

Tang, C., Chen, C., Xu, W., and Xu, L. (2019). Design of doped cesium lead halide perovskite as a photo-catalytic CO 2 reduction catalyst. *J. Mat. Chem. A Mat.* 7, 6911–6919. doi:10.1039/c9ta00550a

Wang, Q., Tao, L., Jiang, X., Wang, M., and Shen, Y. (2019). Graphene oxide wrapped $CH_3NH_3PbBr_3$ perovskite quantum dots hybrid for photoelectrochemical CO_2 reduction in organic solvents. *Appl. Surf. Sci.* 465, 607–613. doi:10.1016/j.apsusc.2018.09.215

Wang, J.-C., Li, N., Idris, A. M., Wang, J., Du, X., Pan, Z., et al. (2021). Surface defect engineering of $CsPbBr_3$ nanocrystals for high efficient photocatalytic CO_2 reduction. *Sol. RRL* 5, 2100154. doi:10.1002/solr.202100154

Wang, C., Li, S., Cai, M., Yan, R., Dong, K., Zhang, J., et al. (2022). Rationally designed tetra (4-carboxyphenyl) porphyrin/graphene quantum dots/bismuth molybdate Z-scheme heterojunction for tetracycline degradation and Cr(VI) reduction: Performance, mechanism, intermediate toxicity appraisement. *J. Colloid Interface Sci.* 619, 307–321. doi:10.1016/j.jcis.2022.03.075

Wei, K., Faraj, Y., Yao, G., Xie, R., and Lai, B. (2021). Strategies for improving perovskite photocatalysts reactivity for organic pollutants degradation: A review on recent progress. *Chem. Eng. J.* 414, 128783. doi:10.1016/j.cej.2021.128783

Xu, Y.-F., Yang, M.-Z., Chen, B.-X., Wang, X.-D., Chen, H.-Y., Kuang, D.-B., et al. (2017). A $CsPbBr_3$ perovskite quantum dot/graphene oxide composite for photocatalytic CO_2 reduction. *J. Am. Chem. Soc.* 139, 5660–5663. doi:10.1021/jacs.7b00489

Yang, D., Cao, M., Zhong, Q., Li, P., Zhang, X., and Zhang, Q. (2019). All-inorganic cesium lead halide perovskite nanocrystals: Synthesis, surface engineering and applications. *J. Mat. Chem. C Mat.* 7, 757–789. doi:10.1039/c8tc04381g

Zhang, H., Feng, J., Wang, J., and Zhang, M. (2007). Preparation of ZnO nanorods through wet chemical method. *Mater. Lett.* 61, 5202–5205. doi:10.1016/j.matlet.2007.04.030

Zhang, Q., Tai, M., Zhou, Y., Zhou, Y., Wei, Y., Tan, C., et al. (2019). Enhanced photocatalytic property of γ-$CsPbI_3$ perovskite nanocrystals with WS_2. *ACS Sustain. Chem. Eng.* 8, 1219–1229. doi:10.1021/acssuschemeng.9b06451

Zhang, L., Liu, Y., He, Y., Zhang, X., Geng, C., Yang, R., et al. (2021a). Stable $CsPbX_3$/ZnO Heterostructure nanocrystals for light-emitting application. *J. Phys. Chem. Lett.* 12, 10953–10957. doi:10.1021/acs.jpclett.1c03446

Zhang, Y., Liu, X., Yusoff, M., and Razali, M. H. (2021b). Photocatalytic and antibacterial properties of a 3D flower-like TiO2 nanostructure photocatalyst.*Scanning*, 2021, 3839235, doi:10.1155/2021/3839235

Zhao, G., Rui, K., Dou, S. X., and Sun, W. (2018). Heterostructures for electrochemical hydrogen evolution reaction: A review. *Adv. Funct. Mat.* 28, 1803291. doi:10.1002/adfm.201803291

Zhao, Y., Shi, H., Hu, X., Liu, E., and Fan, J. (2020). Fabricating $CsPbX_3$/CN heterostructures with enhanced photocatalytic activity for penicillins 6-APA degradation. *Chem. Eng. J.* 381, 122692. doi:10.1016/j.cej.2019.122692

Zhao, Y., Wang, C., Hu, X., and Fan, J. (2021). Recent progress in $CsPbX_3$ perovskite nanocrystals for enhanced stability and photocatalytic applications. *ChemNanoMat* 7, 789–804. doi:10.1002/cnma.202100094